VIP Water Oxidation Catalysts | Very Important Paper

DOI: 10.1002/anie.201307543

Active Mixed-Valent MnO_x Water Oxidation Catalysts through Partial Oxidation (Corrosion) of Nanostructured MnO Particles**

Arindam Indra, Prashanth W. Menezes, Ivelina Zaharieva, Elham Baktash, Johannes Pfrommer, Michael Schwarze, Holger Dau, and Matthias Driess**

Dedicated to Professor Bernt Krebs on the occasion of his 75th birthday

Conversion of solar to chemical energy in natural photosynthesis is the most abundant and sustainable source of energy production. As a central part of the latter process, the oxidation of water to oxygen, which is a four-electron and four-proton transfer process, takes place in the photosystem II (PS II) at the oxygen evolving centers (OEC) of Mn_4Ca clusters.[1]

Although there have been substantial developments in revealing the structural and functional motifs of PS II by various spectroscopic techniques and X-ray crystallography, the resolution acquired by these methods were insufficient to recognize crucial features. Recently, Umena et al. solved the crystal structure of PS II at unprecedented resolution (1.9 Å) with $CaMn_4O_5$ units as the OEC ligated with the highly conserved amino acids environment,[2] which is closely related to the structure reported by Dau et al. by EXAFS analysis.[3] In the $CaMn_4$ cluster, five oxygen atoms serve as oxido bridges to the metal centers to form a distorted $CaMn_3O_4$ cubane with an additional Mn site. Theoretical and computational studies based on the $CaMn_4O_5$ subunit could also elucidate the spectroscopic, magnetic, and functional properties of PS II.[4]

Homogeneous biomimicking manganese-containing model complexes have been known for a long time,[5–8] whereas respective heterogeneous functional analogues have only been uncovered and modified in recent years.[9] Kurz et al. reported the calcium manganate(III) hydrates, $CaMn_2O_4{\cdot}xH_2O$, with high surface areas for photochemical water oxidation.[10,11] Efficient water oxidation employing layered anionic manganese oxo frameworks with intercalated alkali metal counterions has also been reported by the same group.[12] Water oxidation using amorphous binary manganese oxides of octahedral molecular sieves was studied by Suib et al.[13] Frei et al. have used mesoporous silica (KIT-6) supported manganese oxide catalysts for water oxidation,[14a,b] while very recently, Nepal and Das described the successful heterogenization of an active molecular manganese(III) bis(μ-oxido) manganese(IV) catalyst in MOF pores (MOF = metal–organic framework).[14c]

Electrodeposited manganese oxides for electrochemical water oxidation at comparatively high rates have been examined by Zaharieva, Dau, et al.[15] employing X-ray absorption spectroscopy (XAS); it was shown that for effective water oxidation the oxidation state of manganese in the amorphous catalyst varies from 3.5–3.8,[15] in line with recent results of Yano, Jaramillo, et al.[16] Spiccia et al. modeled a geochemical conversion cycle involving a water-oxidizing $Mn^{III,IV}$ oxide as well as studying screen-printed MnO_x films.[17] Recently, Dismukes et al. reported that active water oxidation manganese oxide catalysts containing Mn^{III} sites with longer Mn–O bonds between edge-sharing MnO_6 octahedra.[18] The previous results prompted us to investigate whether suitable heterogeneous mixed-valent MnO_x catalysts are accessible through stepwise partial oxidation (corrosion) of well-defined but catalytically inactive MnO nanoparticles by employing molecular oxidants. In fact, we learned that mixed-valent amorphous MnO_x catalysts suitable for the photochemical and electrochemical water oxidation can be easily synthesized starting from nanostructured MnO precursors and ceric ammonium nitrate (CAN) as an oxidant. To the best of our knowledge, this is the first report of MnO being employed as a precursor for the preparation of an active MnO_x water oxidation catalyst. Our corrosion approach demonstrates that neutral active layered MnO_x structures can be prepared without the presence of alkali and/or alkaline earth metal cations.

The nanostructured MnO precursor was synthesized from Mn^{II} acetate in the presence of tri-*n*-octylphosphine oxide (TOPO) and benzylamine in a sealed tube (see the Experimental Section and Scheme 1). The physical properties of the as-prepared MnO particles were investigated using various analytical techniques, including powder X-ray diffraction (PXRD), scanning electron microscopy with X-ray energy dispersive spectroscopy (SEM/EDX), transmission electron microscopy (TEM), X-ray photoelectron spectroscopy (XPS), nitrogen adsorption and desorption (BET specific surface), and infrared spectroscopy (IR; see the Supporting Informa-

[*] Dr. A. Indra, Dr. P. W. Menezes, E. Baktash, J. Pfrommer, Dr. M. Schwarze, Prof. Dr. M. Driess
Institut für Chemie: Metallorganische Chemie und Anorganische Materialien, Technische Universität Berlin
Strasse des 17 Juni 135, Sekr. C2, 10623 Berlin (Germany)
E-mail: matthias.driess@tu-berlin.de
Dr. I. Zaharieva, Prof. Dr. H. Dau
Fachbereich Physik, Freie Universität Berlin
Arnimallee 14, 14195 Berlin (Germany)
E-mail: holger.dau@fu-berlin.de

[**] Financial support by the BMBF (L2H project) and the DFG (Cluster of Excellence UniCat and SPP1613) is gratefully acknowledged. We thank Dr. A. Knop-Gericke and Prof. Dr. R. Schlögl (Fritz Haber Institute, Berlin) for XPS, and Dr. P. Chernev and J. Heidkamp (FU Berlin) for XAS data collection.

Supporting information for this article is available on the WWW under http://dx.doi.org/10.1002/anie.201307543.

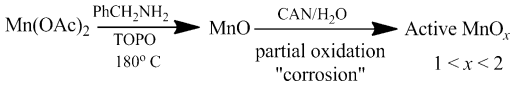

Scheme 1. Synthesis of the active MnO_x water oxidation catalyst through partial oxygenation of nanostructured MnO with Ce^{4+} as oxidant.

tion (SI) for further analytical details). The PXRD pattern revealed that the as-prepared MnO crystallizes in the cubic system with (111), (200), (220), (311), and (222) crystal faces (SI, Figure S1). The scanning electron microscopy (SEM) analysis of MnO showed cubical-shaped particles with sizes ranging from 40 to 80 nm (SI, Figure S2). High-resolution transmission electron microscopy (HRTEM) analysis revealed the presence of a thin amorphous layer on the surface of the cubical-shaped particles (Figure 1). Characteristic Mn–O vibrations were observed in the IR spectrum (SI, Figure S3).

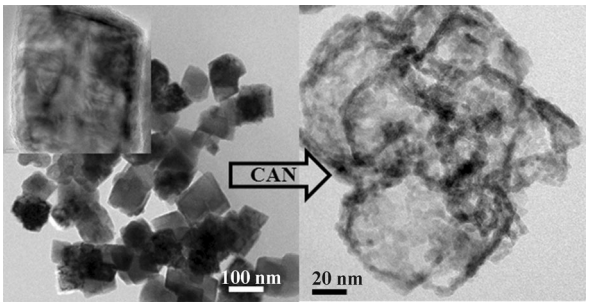

Figure 1. HR-TEM images of as-prepared MnO (left) and active MnO_x (right) after treatment with ceric ammonium nitrate (CAN). The amorphous layer at the surface of crystalline MnO is shown in inset of the left image.

The well-defined MnO precursor was used for chemical oxidation of water in the presence of 0.5 M CAN solutions as oxidant. The amount of evolved oxygen was measured by the Clark electrode and is comparable to the values reported for other manganese oxide based catalysts (SI, Figure S4).[9–12] The rate of the oxygen evolution of 0.07 $mmol(O_2)\,mol(Mn)^{-1}\,s^{-1}$ was determined from the slope of the linear fitting for the first 60 s. A closer look at the concentration profiles of evolved oxygen versus time revealed that the reaction was rather slower at the outset by the appearance of an induction time before the oxygen evolution. The reaction becomes accelerated only after seven seconds of adding CAN. This observed induction time can be attributed to the time required for the transformation of the catalytically inactive MnO precursor to the active MnO_x catalyst.

Furthermore, we tested the as-prepared active MnO_x catalyst for chemical water oxidation and observed that the amount of evolved oxygen was more than twice of MnO within the first 3 min of reaction. The increment in the rate of oxygen evolution followed the similar trend to that of MnO with the value 0.16 $mmol(O_2)\,mol(Mn)^{-1}\,s^{-1}$. No distinct induction time was observed for the active MnO_x catalyst, indicating that the transformed MnO_x is sufficiently active to initiate the water oxidation.

As stated above, effective water oxidation likely requires the presence of Mn sites with a mean Mn oxidation state between 3.5 and 3.8. The conversion of inactive MnO to catalytically active MnO_x by the treatment with CAN is accomplished by the increase in the oxidation state of some of the Mn^{II} centers to Mn^{III} and Mn^{IV} sites. With these initial results in hand, we have extensively characterized the resulting active MnO_x catalysts and compared them with the MnO precursor. In the PXRD pattern, it can clearly be seen that the main crystallinity of MnO is lost after CAN treatment; affording largely amorphous MnO_x materials (SI, Figure S1).

Conversion of the cubical-shaped MnO-nanoparticles suspended in water through treatment with CAN led to amorphous hollow cubes as proven by TEM investigations (Figure 1). Brunauer–Emmett–Teller (BET) analysis of the latter sample shows a remarkable increase in the surface area from 28 $m^2\,g^{-1}$ for MnO precursor to 88 $m^2\,g^{-1}$ for the active MnO_x material. The increase in oxidation state of manganese in active MnO_x was shown by X-ray photoelectron spectroscopy (XPS) studies, which revealed an increase in Mn $2p_{3/2}$ and $2p_{1/2}$ binding energy by 0.29 eV (SI, Figure S5).

The increase in the oxidation state of MnO after the CAN treatment was confirmed by an X-ray absorption near-edge structure (XANES) study (at the BESSY synchrotron operated by the Helmholtz Zentrum Berlin). Mn K-edge X-ray absorption spectroscopic studies showed an increase in absorption energy after the CAN treatment. Comparison of the edge-position energy to that of typical standard Mn oxides with known oxidation states[19] established that there was an enhancement in the mean oxidation state of Mn from +2 to about +2.5, after 15 min of CAN treatment (SI, Figure S6). This overall oxidation state is still lower than typical values for high-valent manganese oxides (>3) and indicates that not all Mn ions have been propelled to higher oxidation states by using Ce^{IV} as an oxidant.

The intermediate oxidation state after CAN treatment could be explained in two ways: 1) A core–shell model, where surface layers of Mn^{II} ions of the precursor are oxidized to Mn^{III} and/or Mn^{IV} sites; and 2) the structural rearrangement of the complete MnO precursor to the active catalyst possibly involving incorporation of cerium. Incorporation of cerium into the structure of the active catalyst could be ruled out by results of energy dispersive X-ray (EDX) analysis (SI, Figure S7). For further clarification, the direct structural aspects and the oxidation states of Mn in active MnO_x catalyst were analyzed by EXAFS studies. Figure 2 shows the experimental EXAFS spectra and the simulated spectra of MnO and active MnO_x. For the MnO precursor, spectra and distances (SI, Table S1) confirm and extend the PXRD results by showing that the bulk material consists of MnO, without any detectable contribution of further (amorphous) Mn-oxide phases.

A severe structural rearrangement was observed for MnO_x. Simulation of the spectra was performed with two oxygen shells, and with seven Mn–Mn distances (SI, Table S1). The first Mn–O distance (1.9 Å) is typical for

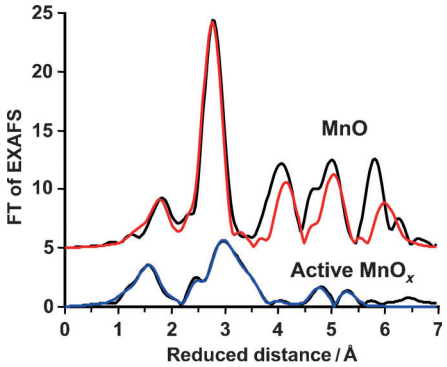

Figure 2. Fourier-transformed EXAFS spectra (black line) and the simulated spectra (colored line) of MnO and active MnO_x. The deviation between simulated and experimental spectrum of the MnO precursor at higher distances is due to the strong multiple-scattering contributions expected for this highly symmetric structure, which were not taken into account in the simulations.

Mn^{IV}–O or Mn^{III}–O in the equatorial plane of Jahn–Teller elongated Mn^{III},[20] and the second (2.3 Å), for Mn^{II}–O.[21] The longer Mn–O distance can also be attributed to Jahn–Teller elongated Mn^{III}–O bonds (species with $t_{2g}^3e_g^1$ electronic configuration in octahedral environment).[18]

For the active MnO_x, several Mn–Mn distances match distances detected previously in water-oxidizing $Mn^{III,IV}$ oxides.[11,12,15] The Mn–Mn distance of 2.9 Å is indicative of di-μ-oxido bridging between high-valent $Mn^{III,IV}$ ions (edge-sharing MnO_6 octahedra). Also other Mn–Mn distance of 3.4 Å, 3.8 Å, and 5.6 Å present in the active MnO_x have been found previously in water-oxidizing Mn oxides. Thus a sizeable fraction (25–50 %) of the active MnO_x likely consists of an amorphous phase, which resembles the previously described water-oxidizing Mn oxides closely. Based on this similarity, a structural model of the catalytically active phase of MnO_x is proposed which is illustrated by Figure 3 and described in the following: Layers of di-μ-oxido bridged Mn ions as found in birnesites or buserites[22] represent the parent structure of the water-oxidizing phase in MnO_x. The space between these oxide layers (or rather layer fragments) is occupied by water molecules and cations. In the MnO_x investigated herein, the interlayer cations are either Mn^{II} or Mn^{III}, whereas in water-oxidizing Mn-Ca/Sr/Mg/K oxides these are alkali or alkaline earth metals.[11,12,15] The interlayer cations are bound by via μ-oxido bridges to the layered-oxide fragments as shown in Figure 3.

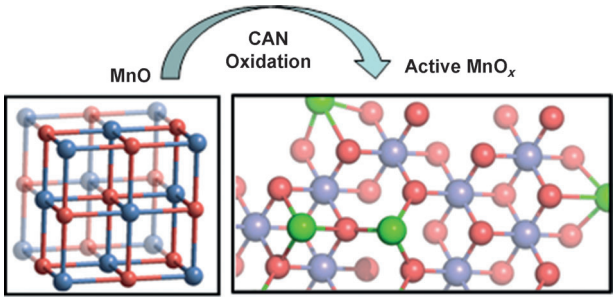

Figure 3. Representative structural cutout of the crystalline MnO precursor and the mixed-valent oxide of the active MnO_x catalyst as deduced from EXAFS analyses. Right: The Mn atoms in violet form a defect-rich layer of di-μ-oxido bridged $Mn^{III,IV}$ ions; the $Mn^{II,III}$ ions in green are not part of this layer and may interconnect layer fragments. In water-oxidizing Mn-Ca oxides, Ca ions occupy the interlayer positions indicated in green.

The EXAFS analysis also revealed the presence of Mn–Mn distances of 3.1 Å and 4.4 Å in both the MnO precursor and the active MnO_x, suggesting that a largely amorphous Mn^{II} phase is formed which is structurally related to the MnO parent structure. Thus, the average oxidation state of about +2.5 found for the active MnO_x is explainable by having, in addition to the $Mn^{III,IV}$ oxide described above, an amorphous Mn^{II} phase, which involves 50–75 % of the Mn ions. In summary, the determined metric changes indicate that upon CAN treatment, the initial MnO structure was converted and reorganized into an amorphous oxide containing a catalytically active $Mn^{III,IV}$ oxide.

The ability of the active MnO_x catalyst for photochemical water oxidation was tested in the presence of $[Ru(bpy)_3]^{2+}$ photosensitizer to mimic light-driven water oxidation in PS II. A negligible amount of oxygen evolution was observed for the MnO precursor sample (Figure 4). However, a significant

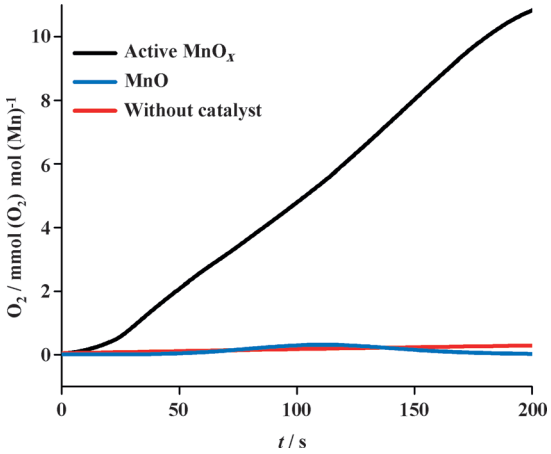

Figure 4. Oxygen evolution profiles for the photochemical water oxidation with $[Ru(bpy)_3]^{2+}$ as photosensitizer.

amount of oxygen evolution can be detected for the active MnO_x, which indeed shows that the catalyst is active for the photochemical water oxidation. Interestingly, this also means that biomimicking heterogeneous manganese oxides can show efficient water oxidation in the absence of calcium or any other alkali and alkaline-earth metals. $H_2{}^{18}O$ labeling studies on active MnO_x further proved that the oxygen was generated from water (SI, Table S2) and not from any other sources.

The moderate increase in surface area upon CAN treatment of the MnO nanoparticles (28 to 88 $m^2 g^{-1}$) cannot explain the transformation from a material virtually inactive in photochemical water oxidation towards an active catalyst. Decisive is probably the formation of a disordered high-valent oxide containing Mn^{III} ions aside from Mn^{IV}, in line with results from recent investigations on MnCa oxides[11] and

electrodeposited Mn oxides.[15] Previously, Morita et al. have observed that the manganese oxides used for electrocatalysis showed better catalytic activities with Mn^{III} species compared to pure MnO_2.[23] Recently, Dismukes et al. have studied a series of high-valent manganese oxide catalysts for the water oxidation and found that the Mn^{III} species with the longer Mn–O bonds between edge-sharing MnO_6 octahedra may be crucial for effective water oxidation.[18] Disorder, that is, defects and vacancies in the structure of manganese oxides, promote the activity also for the electrocatalytic oxygen reduction reaction (ORR).[24]

The promising use of the active MnO_x for photochemical water oxidation prompted us to approach deposition on electrode surfaces and electrochemical investigation. (We note in passing that catalyst deposition on electrode or semiconductor surfaces is of high importance regarding use as co-catalyst on photoelectrodes in devices for light-driven water splitting.) Indium tin oxide (ITO)-deposited thin films of active MnO_x have been prepared and characterized by SEM analysis. The thickness of the film was determined to be 190 nm (SI, Figure S8a). Figure 5 shows the cyclic voltammogram at pH 7.0 in an aqueous phosphate buffer. The anodic current started growing at 1.25 V (vs. the normal hydrogen electrode, NHE) and the current density reached 900 μA at 1.4 V (Tafel slope is 120 mV dec^{-1}). The remarkably high stability of the MnO_x film was verified by three repetitive scans under semi-stationary condition where the potential was changed with only 2 mV s^{-1} (SI, Figure S9a). Despite the high functional stability, the SEM characterization of the films after electrochemical measurement shows substantial agglomeration of the particles (SI, Figure S8b). Long-term controlled-potential electrolysis in 0.1M potassium phosphate solution (pH 7) was conducted at 1.3 V vs. NHE, which corresponds to an overpotential of 485 mV (SI, Figure S9b). The catalytic performance resulted here was highly comparable or even larger than the previously reported values obtained under similar conditions.[15,25]

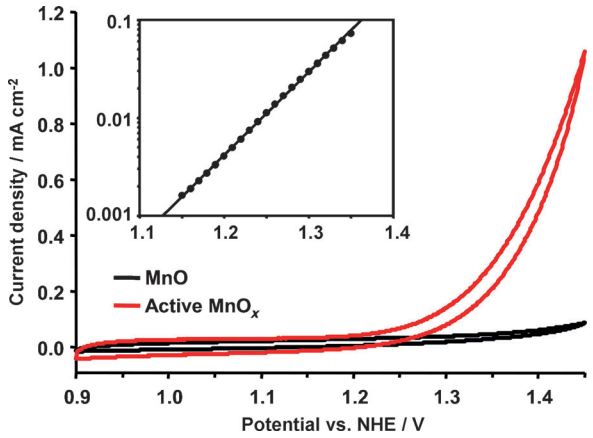

Figure 5. Cyclic voltammograms of the active MnO_x vs. inactive MnO films in 0.1 M phosphate buffer at pH 7 with sweep rate of 20 mV s^{-1}. Inset: Tafel plot (log[current density] vs. potential) of the active MnO_x thin film (slope of 120 mV dec^{-1}).

After the successful use of the mixed-valent amorphous active MnO_x as water-oxidation catalysts, we decided to generalize the novel synthetic route to prepare MnO from other manganese precursors and to test their activity for chemical and photochemical water oxidation. Following the same preparation conditions for MnO from $Mn(OAc)_2$, we also synthesized and characterized MnO-1 from $[Mn(acac)_2]$ (acac = acetylacetonate; SI, Figures S10–S14). The SEM analysis of the latter revealed that the particles have a spherical shape (SI, Figure S10). The particle size determined from TEM studies was in the range of 10–20 nm (SI, Figure S11). After the CAN treatment, the spherical MnO-1 was converted into amorphous active MnO_x-1 as revealed from PXRD pattern (SI, Figure S12) as well as TEM analysis. The increase in surface area was larger after the CAN treatment of MnO-1 (from 34 for MnO-1 to 188 $m^2 g^{-1}$ for active MnO_x-1) than that observed for MnO.

Remarkably, the chemical and the photochemical water oxidation catalyzed by MnO_x-1 shows improved catalytic activities in comparison with that of the aforementioned active MnO_x (SI, Figures S15, S16). The higher activity of MnO_x-1 demonstrates the potential for improved catalytic performance and can be explained by the higher surface area of the materials. Further development in the synthesis of high-surface-area amorphous MnO_x water-oxidation catalysts by partial oxidation of a MnO precursor is currently in progress. The proposed corrosion approach was also applied to the other oxidizing agents such as dichromate, ruthenium trichloride, and hydrogen peroxide. Thermodynamically, dichromate and ruthenium trichloride are unfeasible, whereas hydrogen peroxide has the suitable potential to convert Mn^{II} into Mn^{III}/Mn^{IV} species. Treatment of MnO cubes with the hydrogen peroxide also produced amorphous material (SI, Figures S17, S18) and showed lower activity in photochemical water oxidation in comparison to the active MnO_x.

In conclusion, we report for the first time the unexpected facile conversion of catalytically inactive nanostructured MnO precursors into active amorphous MnO_x catalysts for effective water oxidation by using ceric ammonium nitrate (CAN) as an oxidant (corrosion agent). The effective photochemical water oxidation of the active catalysts has been carried out in the presence of $[Ru(bpy)_3]^{2+}$ as a photosensitizer. Structural characterization of the active MnO_x catalyst by XAS revealed the presence of Mn^{II}, Mn^{III}, and Mn^{IV} sites. A series of defects and structural disorder in the di-μ-oxido-bridged structure makes the catalyst analogous to calcium–manganese oxide systems, but the calcium sites are occupied by Mn^{II} or Mn^{III} ions. In other words, the structural motif of the active MnO_x catalyst is close to biomimetic water oxidation catalyst systems, which explains its efficient catalytic activity in water oxidation.

Experimental Section

Synthesis of the MnO precursor: A mixture of tri-*n*-octylphosphine oxide (4 mmol, 1.55 g) and dry benzylamine (10 mL) in a glass tube was heated at 60 °C for 5 min in N_2 flush. Manganese acetate (4 mmol, 692 mg) was then added to the above mixture and was slowly heated to 80 °C in flushing N_2 and kept at this temperature for 1 hour. A

reddish brown solution was obtained. The glass tube was sealed in N_2 atmosphere and placed in an oil bath preheated at 180 °C. After 3 h, the tube was removed from the oil bath and cooled down to room temperature. 10 mL of a methanol/chloroform (1:1) mixture was added to the obtained product and was aged overnight. Thus obtained brownish solid precipitate was washed several times with methanol/chloroform mixture before drying in air at 50 °C for 12 h. The yield of the isolated product varied from 64–70 %.

Synthesis of active MnO_x catalyst: 50 mg MnO was treated with 25 mL of 0.5 M ceric ammonium nitrate (CAN) solution for 15 min with vigorous stirring. The solid material was centrifuged and washed several times with water, finally with ethanol, and dried overnight at 50 °C to form MnO_x.

Received: August 27, 2013
Published online: October 31, 2013

Keywords: electrochemistry · metal oxide catalysis · oxygen evolution reaction · photochemistry · water splitting

[1] a) J. P. McEvoy, G. W. Brudvig, *Chem. Rev.* **2006**, *106*, 4455 – 4483; b) H. Dau, M. Haumann, *Coord. Chem. Rev.* **2008**, *252*, 273 – 295; c) H. Dau, C. Limberg, T. Reier, M. Risch, S. Roggan, P. Strasser, *ChemCatChem* **2010**, *2*, 724 – 761.
[2] Y. Umena, K. Kawakami, J. R. Shen, N. Kamiya, *Nature* **2011**, *473*, 55 – 60.
[3] H. Dau, A. Grundmeier, P. Loja, M. Haumann, *Philos. Trans. R. Soc. London Ser. B* **2008**, *363*, 1237 – 1244.
[4] a) V. Krewald, F. Neese, D. A. Pantazis, *J. Am. Chem. Soc.* **2013**, *135*, 5726 – 5739; b) E. M. Sproviero, J. A. Gascon, J. P. Mcevoy, G. W. Brudvig, V. S. Batista, *J. Am. Chem. Soc.* **2008**, *130*, 6728 – 6730; c) P. E. M. Siegbahn, *Acc. Chem. Res.* **2009**, *42*, 1871 – 1880; d) S. Schinzel, J. Schraut, A. V. Arbuznikov, P. E. M. Siegbahn, M. Kaupp, *Chem. Eur. J.* **2010**, *16*, 10424 – 10438.
[5] S. Mukhopadhyay, S. K. Mandal, S. Bhaduri, W. H. Armstrong, *Chem. Rev.* **2004**, *104*, 3981 – 4026.
[6] K. Wieghardt, *Angew. Chem.* **1989**, *101*, 1179 – 1198; *Angew. Chem. Int. Ed. Engl.* **1989**, *28*, 1153 – 1172.
[7] C. S. Mullins, V. L. Pecoraro, *Coord. Chem. Rev.* **2008**, *252*, 416 – 443.
[8] G. Christou, *Acc. Chem. Res.* **1989**, *22*, 328 – 335.
[9] a) M. Wiechen, H. M. Berends, P. Kurz, *Dalton Trans.* **2012**, *41*, 21 – 31; b) M. M. Najafpour, B. Pashaei, *Dalton Trans.* **2012**, *41*, 10156 – 10160; c) M. M. Najafpour, *Dalton Trans.* **2011**, *40*, 3805 – 3807; d) D. M. Robinson, Y. B. Go, M. Greenblatt, G. C. Dismukes, *J. Am. Chem. Soc.* **2010**, *132*, 11467 – 11469.
[10] M. M. Najafpour, T. Ehrenberg, M. Wiechen, P. Kurz, *Angew. Chem.* **2010**, *122*, 2281 – 2285; *Angew. Chem. Int. Ed.* **2010**, *49*, 2233 – 2237.
[11] I. Zaharieva, M. M. Najafpour, M. Wiechen, M. Haumann, P. Kurz, *Energy Environ. Sci.* **2011**, *4*, 2400 – 2408.
[12] M. Wiechen, I. Zaharieva, H. Dau, P. Kurz, *Chem. Sci.* **2012**, *3*, 2330 – 2339.
[13] A. Iyer, J. D. Pilar, C. K. Kingondu, E. Kissel, H. F. Garces, H. Huang, M. A. El-Sawy, P. K. Dutta, S. L. Suib, *J. Phys. Chem. C* **2012**, *116*, 6474 – 6483.
[14] a) F. Jiao, H. Frei, *Energy Environ. Sci.* **2010**, *3*, 1018 – 1027; b) F. Jiao, H. Frei, *Chem. Commun.* **2010**, *46*, 2920 – 2922; c) B. Nepal, S. Das, *Angew. Chem.* **2013**, *125*, 7365 – 7368; *Angew. Chem. Int. Ed.* **2013**, *52*, 7224 – 7227.
[15] I. Zaharieva, P. Chernev, M. Risch, K. Klingan, M. Kohlhoff, A. Fischer, H. Dau, *Energy Environ. Sci.* **2012**, *5*, 7081 – 7089.
[16] Y. Gorlin, B. L. -Kaiser, J. D. Benck, S. Gul, S. M. Webb, V. K. Yachandra, J. Yano, T. F. Jaramillo, *J. Am. Chem. Soc.* **2013**, *135*, 8525 – 8534.
[17] a) R. K. Hocking, R. Brimblecombe, L. Y. Chang, A. Singh, M. H. Cheah, C. Glover, W. H. Casey, L. Spiccia, *Nat. Chem.* **2011**, *3*, 461 – 466; b) M. Fekete, R. K. Hocking, S. L. Y. Chang, C. Italiano, A. F. Patti, F. Arena, L. Spiccia, *Energy Environ. Sci.* **2013**, *6*, 2222 – 2232.
[18] D. M. Robinson, Y. B. Go, M. Mui, G. Gardner, Z. Zhang, D. Mastrogiovanni, E. Garfunkel, J. Li, M. Greenblatt, G. C. Dismukes, *J. Am. Chem. Soc.* **2013**, *135*, 3494 – 3501.
[19] H. Dau, P. Liebisch, M. Haumann, *Anal. Bioanal. Chem.* **2003**, *376*, 562 – 583.
[20] R. W. G. Wyckoff, *Crystal Structures 1*, Interscience, New York, **1963**, pp. 239 – 444.
[21] R. E. Pacalo, E. K. Graham, *Phys. Chem. Miner.* **1991**, *18*, 69 – 80.
[22] J. E. Post, *Proc. Natl. Acad. Sci. USA* **1999**, *96*, 3447 – 3454.
[23] M. Morita, C. Iwakura, H. Tamura, *Electrochim. Acta* **1979**, *24*, 357 – 362.
[24] T. Zhang, Y. Zhang, J. Du, X. Han, J. Chen, *Angew. Chem.* **2013**, *125*, 2534 – 2537; *Angew. Chem. Int. Ed.* **2013**, *52*, 2474 – 2477.
[25] M. M. Najafpour, B. Haghighi, M. Z. Ghobadi, D. J. Sedigh, *Chem. Commun.* **2013**, *49*, 8824 – 8826.

